Title

Growth of Myxococcus xanthus in Continuous-Flow-Cell Bioreactors as a Method for Studying Development

Journal

Applied and Environmental Microbiology, 80(8)

ISSN

0099-2240

Authors

Smaldone, Gregory T
Jin, Yujie
Whitfield, Damion L
et al.

Publication Date

2014-04-15

DOI

10.1128/aem.03369-13

Peer reviewed

AEM
Journals.ASM.org

Growth of *Myxococcus xanthus* in Continuous-Flow-Cell Bioreactors as a Method for Studying Development

Gregory T. Smaldone,[a] Yujie Jin,[b] Damion L. Whitfield,[a] Andrew Y. Mu,[a] Edward C. Wong,[c] Stefan Wuertz,[b,d] Mitchell Singer[a]

Department of Microbiology and Molecular Genetics, University of California—Davis, Davis, California, USA[a]; Department of Civil and Environmental Engineering, University of California—Davis, Davis, California, USA[b]; Department of Mechanical and Aerospace Engineering, University of California—Davis, Davis, California, USA[c]; Singapore Centre on Environmental Life Sciences Engineering and School of Civil and Environmental Engineering, Nanyang Technological University, Singapore, Republic of Singapore[d]

Nutrient sensors and developmental timers are two classes of genes vital to the establishment of early development in the social soil bacterium *Myxococcus xanthus*. The products of these genes trigger and regulate the earliest events that drive the colony from a vegetative state to aggregates, which ultimately leads to the formation of fruiting bodies and the cellular differentiation of the individual cells. In order to more accurately identify the genes and pathways involved in the initiation of this multicellular developmental program in *M. xanthus*, we adapted a method of growing vegetative populations within a constant controllable environment by using flow cell bioreactors, or flow cells. By establishing an *M. xanthus* community within a flow cell, we are able to test developmental responses to changes in the environment with fewer concerns for effects due to nutrient depletion or bacterial waste production. This approach allows for greater sensitivity in investigating communal environmental responses, such as nutrient sensing. To demonstrate the versatility of our growth environment, we carried out time-lapse confocal laser scanning microscopy to visualize *M. xanthus* biofilm growth and fruiting body development, as well as fluorescence staining of exopolysaccharides deposited by biofilms. We also employed the flow cells in a nutrient titration to determine the minimum concentration required to sustain vegetative growth. Our data show that by using a flow cell, *M. xanthus* can be held in a vegetative growth state at low nutrient concentrations for long periods, and then, by slightly decreasing the nutrient concentration, cells can be allowed to initiate the developmental program.

In response to limiting nutrient availability, the ubiquitous Gram-negative soil bacterium *Myxococcus xanthus* undergoes a well-characterized developmental program resulting in the differentiation of vegetatively growing cells into one of three cellular fates (1, 2). These cells aggregate to form a macroscopic, multicellular, and rounded fruiting body containing metabolically inactive, stress-resistant myxospores (3, 4). Surrounding the fruiting bodies are peripheral, rod-shaped cells hypothesized to be important in environmental sensing. Lastly, a subpopulation of cells may undergo autolysis, a process suggested to provide nutrients for the other two viable cell fates during differentiation (5, 6).

Expanding our understanding of the complex regulatory networks controlling development has been a major aim since the very first studies of *M. xanthus*. While much progress has been made, much remains unknown, especially those transcriptional changes occurring within the very early stages of nutrient limitation, when the community must make a decision to flip an energy-intensive switch, initiating development. To better understand how and why this occurs, as well as how *M. xanthus* senses nutrient concentrations within the environment, we propose the use of continuous-flow-cell bioreactors, or flow cells, to culture vegetative biofilms.

Growth in an environment that allows for the finite control of inputs and the monitoring of bacterial outputs, such as secondary metabolites and extracellular signals (both small molecules and proteins), is key to understanding how *M. xanthus* senses its surroundings and integrates cues to control growth and development. Due to the tendency of *M. xanthus* to flocculate and stick to surfaces, the use of a chemostat is not practical. However, growing *M. xanthus* as a biofilm adhering to a solid surface under continuous-medium-flow conditions allows for stricter control of constant environmental parameters. Biofilms have been studied extensively in numerous bacterial systems, including *Pseudomonas aeruginosa*, *Bacillus subtilis*, and *Staphylococcus aureus*, among others (7–12). While biofilms of *M. xanthus* are less well studied, recent work has begun to expand our knowledge of biofilm formation and how it relates to nutrient sensing and development (13–15).

In the work presented here, we demonstrate for the first time the use of flow cells as a method for controlling the growth and development of *M. xanthus*. Our aim is to establish the study of *M. xanthus* within flow cells as an attractive alternative to currently favored growth environments. To do so, we present data that illustrate the versatility of this growth method for many standard assays used in the study of *M. xanthus*. Specifically, we performed time-lapse confocal laser scanning microscopy (CLSM) in conjunction with green fluorescent protein (GFP)-tagged markers to visualize biofilm growth and fruiting body development. Similarly, we employed fluorescence cell staining to visualize the deposition of exopolysaccharide by *M. xanthus* biofilms. Lastly, we carried out a nutrient titration to identify at what concentration

Received 10 October 2013 **Accepted** 3 February 2014
Published ahead of print 7 February 2014
Editor: A. M. Spormann
Address correspondence to Mitchell Singer, mhsinger@ucdavis.edu.
Supplemental material for this article may be found at http://dx.doi.org/10.1128/AEM.03369-13.

doi:10.1128/AEM.03369-13

the developmental program is triggered, ultimately leading the established biofilm to fruiting body formation.

MATERIALS AND METHODS

Strains and growth conditions. *M. xanthus* strain DK1622 was used as the wild-type and parental strain for all subsequent strains (16). DK10547 and DK11239, harboring a *gfp* transcriptional fusion cloned under the control of the *pilA* promoter and a *gfp* transcriptional fusion cloned at the end of the *devR* open reading frame, respectively, were used for the fluorescence microscopy studies as indicated (17, 18). Strain DK4521, harboring a Tn*5lac* fusion expressed in development but without any identified phenotype, was used in the mixing experiment as a nonfluorescent kanamycin-resistant strain (19). *M. xanthus* strains were grown in CTTYE (1% Casitone [Difco, Franklin Lakes, NJ], 0.2% yeast extract [BD, Sparks, MD], 10 mM Tris-HCl [pH 7.6], 1 mM KH_2PO_4, 8 mM $MgSO_4$]) broth or on CTTYE plates containing 1% agar for general cultivation. For the purposes of the nutrient titration experiment, a morpholinepropanesulfonic acid (MOPS)-buffered nutrient medium was adapted from the work of Berleman et al. (20) and renamed CTM for this article, to avoid confusion with CTTYE. *M. xanthus* strains were grown in single-chamber flow cells with 1% CTM (1% Casitone, 10 mM MOPS [pH 7.0], 1 mM KH_2PO_4, 8 mM $MgSO_4$, 1 mM $CaCl_2$) unless otherwise stated.

Flow cell assemblies. Biofilms were grown in stainless steel four-chamber flow cells under continuous-flow conditions (21). A single flow chamber was 4 by 4 by 40 mm and had an internal volume of about 1 ml (including the input and effluent ports). Each continuous-flow system consisted of a growth medium reservoir, peristaltic pump, flow cell, and waste reservoir connected by Tygon tubing (Saint-Gobain S.A., Courbevoie, France). For a diagram of the flow cell setup with exact tube sizing, see Fig. S1A in the supplemental material. The entire system, excluding the peristaltic pump, was autoclaved prior to experimentation. Flow cells were then sealed with UV- and 70% ethanol-sterilized Rinzel plastic microscope coverslips (Electron Microscopy Sciences, Hatfield, PA) by use of Devcon home silicone adhesive (Illinois Tool Works Inc., Riviera Beach, FL).

Preparative single-chamber flow cells were designed in order to obtain sufficient biomass to perform a variety of qualitative and quantitative assays, such as protein and RNA analyses (data not shown). The dimensions of these preparative cells were 60 by 23 by 10.5 cm in order to fit one or two 24- by 60-mm Rinzel plastic microscope coverslips. The internal volume of each sealed single-chamber flow cell was approximately 7.5 ml. Design files were generated using the computer-aided design program AutoCAD (Autodesk Inc., San Rafael, CA) and are available at http://microbiology.ucdavis.edu/singer/ for immediate download and printing on compatible three-dimensional printers. The flow cells were printed on an Objet Eden260V three-dimensional printer using VeroBlackPlus resin, a proprietary acrylic-based polymer (Objet Ltd., Minneapolis, MN; UC Davis Prototype Lab, Biomedical Engineering). For a diagram of a single-coverslip flow cell, see Fig. S2 in the supplemental material.

The single-chamber continuous-flow-cell system consisted of a growth medium reservoir, peristaltic pump, single-chamber flow cell, and waste reservoir connected by Tygon tubing. Flow cells were sealed with Rinzel plastic microscope coverslips by use of Devcon home silicone adhesive and were sterilized by exposure to chlorine gas for at least 3 h. Briefly, the assembled flow cells were placed into a vacuum chamber with a beaker containing 100 ml 6.0% sodium hypochlorite (NaClO), to which 3 ml concentrated HCl was added. The chamber was immediately sealed and exposed for 3 h. The chamber was vented for 1 h in a fume hood, and the sterilized flow cells were stored in sterile plastic petri plates until they were attached to the sterilized input and effluent tubing. The system, excluding the peristaltic pump and single-chamber flow cell, was autoclaved prior to experimentation. For a diagram of the flow cell setup with exact tube sizing, see Fig. S1B in the supplemental material.

Biofilm growth for developmental assays and observation. Starter cultures were grown with a large inoculating loopful of the indicated *M. xanthus* strain taken from a fresh 1% CTTYE plate with appropriate antibiotic and inoculated into 25 ml 1% CTTYE broth plus appropriate antibiotic in a 250-ml flask. The culture flask was shaken overnight at 32°C and grown to a Klett measurement of approximately 80 to 100. The culture was pelleted and washed with MC7 buffer (10 mM MOPS [pH 7.0], 1 mM KH_2PO_4, 8 mM $MgSO_4$, and 1 mM $CaCl_2$), and approximately 10^7 cells were inoculated into the flow cell chambers in a volume of 0.25 ml, using a 1-ml syringe with a 25-gauge by 5/8-in. hypodermic needle. A continuous flow of 1% CTTYE medium plus appropriate antibiotic was turned on, at a rate of 2 ml/h, after inoculated cells were allowed to statically adhere to the coverslips for 2 h. Dense microbial mats were allowed to form for 4 to 5 days. The *M. xanthus* developmental program was initiated by rapid buffer exchange with the nutrient-deficient buffer MC7 plus appropriate antibiotic. Images of the developmental program were taken at the indicated time points via CLSM as described below.

Nutrient titration of established biofilms. Starter cultures were grown with a large loopful of either *M. xanthus* wild-type DK1622 or DK11239 taken from a fresh 1% CTTYE plate and inoculated into 25 ml 1% CTTYE in a 250-ml flask. The culture flask was shaken overnight at 32°C and grown to a Klett measurement of approximately 80 to 100. The culture was pelleted and washed with MC7 buffer, and approximately 10^7 cells were inoculated into the flow cell chambers in a volume of 0.75 ml, using a 1-ml syringe with a 25-gauge by 5/8-in. hypodermic needle. Continuous 1% CTM medium flow was turned on, at a rate of 3 ml/h, after inoculated cells were allowed to statically adhere to the coverslips for 2 h. Dense microbial mats were allowed to form for 2 or 3 days. The titration was initiated by a rapid exchange to CTM with the indicated Casitone concentration. Continuous medium flow was carried out for 4 days post-nutritional shift, at 3 ml/h. Cultures were imaged with both a Leica DMI 6000 wide-field inverted fluorescence microscope with a PlanApo 100× (total magnification) objective and a Nikon SMZ800 microscope with a total magnification of ×30.

Biofilm and fruiting body staining. Biofilms were stained under continuous flow for 1 h and then washed with 10 mM $MgSO_4$ for 30 min. Cells were then stained with 5 μM Syto60 (Molecular Probes, Eugene, OR) suspended in 10 mM $MgSO_4$. Extracellular polysaccharide (EPS) was stained with 0.05% (by weight) Solophenyl flavine (SPF; Huntsman Int. LLC, High Point, NC) suspended in 10 mM $MgSO_4$ and filtered using a 0.2-μm sterilization filter (Pall Life Sciences, Port Washington, NY). Images were taken via CLSM as described below.

Development strain mixing assay. Starter cultures were grown with a large loopful of either *M. xanthus* DK10547 or DK4521 taken from a fresh 1% CTTYE plate and inoculated into 25 ml 1% CTTYE in a 250-ml flask. Each culture flask was shaken overnight at 32°C and grown to a Klett measurement of approximately 100 to 200. Both strains were spun down and resuspended in MC7 buffer to a common concentration of 100 Klett units. The strains were then mixed at either a 1:1 or 1:5 ratio of DK10547 to DK4521. Approximately 10^7 cells from the mixtures were inoculated into the flow cell chambers in a volume of 0.75 ml by using a 1-ml syringe with a 25-gauge by 5/8-in. hypodermic needle. Continuous 1% CTM medium flow was turned on, at a rate of 3 ml/h, after inoculated cells were allowed to statically adhere to the coverslips for 2 h. Dense microbial mats were allowed to form for 3 days. The *M. xanthus* developmental program was initiated by a rapid exchange to the nutrient-deficient buffer MC7. Continuous buffer flow was carried out for 3 days post-nutritional shift, at 3 ml/h. Cultures were imaged at that time, using a Leica DMI 6000 wide-field inverted fluorescence microscope with a PlanApo 100× (total magnification) objective. GFP intensity was determined by ImageJ (22), using three independent measurements of fruiting body fore- and background intensities for both ratios tested.

CLSM observation. Stainless steel four-chamber flow cells were mounted on a Zeiss 510 Meta CLSM (Carl Zeiss, Jena, Germany) motorized stage and visualized using a 20× objective lens. The biofilm was scanned using a 488-nm argon laser with a 505-nm-band-pass filter. z-stacks scanned from a single biofilm contained the same number of im-

ages. The number of images was set to capture the thickest part of the biofilm. The z step for images in a z-stack was 1 μm. Images were acquired by utilizing a pinhole setting of 1 airy unit and a scan average of 2. Detector gain (500 to 550 arbitrary units), amplifier offset (0 to 0.05 arbitrary unit), and laser intensity (10% to 25%) were all set to obtain adequately contrasted grayscale images based on the brightest region of the biofilm that was scanned.

Image analysis. Semiautomated image analysis was performed utilizing the programs Auto PHLIP-ML and PHLIP. Auto PHLIP-ML (http://sourceforge.net/projects/auto-phlip-ml/) calculates an Otsu threshold for image stacks not biased by extraneous images (images not containing pixels of biological significance). Extraneous images are identified and removed based on their area coverage of biomass, as described by Merod et al. (23). The percent area coverage value used for extraneous image removal (PACVEIR) identifying the substratum was set at 1%. The bulk-medium interface was defined by the limit of EPS and iteratively determined to be a PACVEIR of either 0% or 0.005%. PHLIP, version 0.7, a MatLab-based image analysis toolbox (http://sourceforge.net/projects/phlip/), was used to quantify architectural metrics for each z-stack. A second method, bioView3D, was also employed to qualitatively visualize and present the architectural structure of each z-stack (24).

RESULTS

Biofilm growth and developmental shifts within flow cells. We monitored the growth and development of *M. xanthus* communities established in continuous-flow cells. Investigations with *Pseudomonas* species have recognized this culturing method as an excellent way to observe vegetative growth and the establishment of higher-order structures within a microbial community (25, 26). Our initial trials were carried out to monitor homogeneous growth on a solid surface. Standard 1% CTTYE broth was used to bathe *M. xanthus* cells statically inoculated into the flow cell onto a plastic coverslip. After attachment, medium flow was turned on, and growth of DK10547 was monitored by CLSM. Vegetative growth was maintained with a high nutrient content for the duration of our observation, i.e., 3 days, producing a dense homogenous biofilm that was readily observable and consistent with previously published studies obtained using a similarly labeled *pilA-gfp* transcriptional fusion strain (Fig. 1A) (27). z-stacks imaged during vegetative growth were analyzed and allowed us to calculate the cell depth in several locations within the biofilm. Using an estimate of 1 μm as the cell diameter, we calculated a maximal cell depth of 50 cells. More importantly, the z-stack images could be used to generate three-dimensional (3D) images of the biofilm to examine biofilm architecture in more detail, using an open-software package called Bisque (24). Using these 3D biofilm images, we observed a dense microbial mat but also the establishment of higher-order structures, such as cell aggregates or possible transient swarms (Fig. 1B). These aggregates can be observed as bright fluorescent patches (Fig. 1A) and as "pebble-like" speckling under a light microscope (see Fig. 4, top row).

After 4 to 5 days of vegetative growth under nutrient-replete conditions, the *M. xanthus* developmental program was initiated by the rapid exchange of nutrient-replete 1% CTTYE with nutrient-depleted MC7 buffer. Development was monitored over the following 4 days, and fruiting body formation was readily observable by both eye and CLSM (Fig. 1C). CLSM images of an *M. xanthus pilA-gfp* fruiting body showed the characteristic halo effect observed by Lux et al., due to the loss of *pilA* expression within the myxospore (28). This can be seen in more detail in the z-stack 3D image depicted in Fig. 1D. The 3D rendering of the fruiting body z-stack compared to the biofilm rendering illustrates a

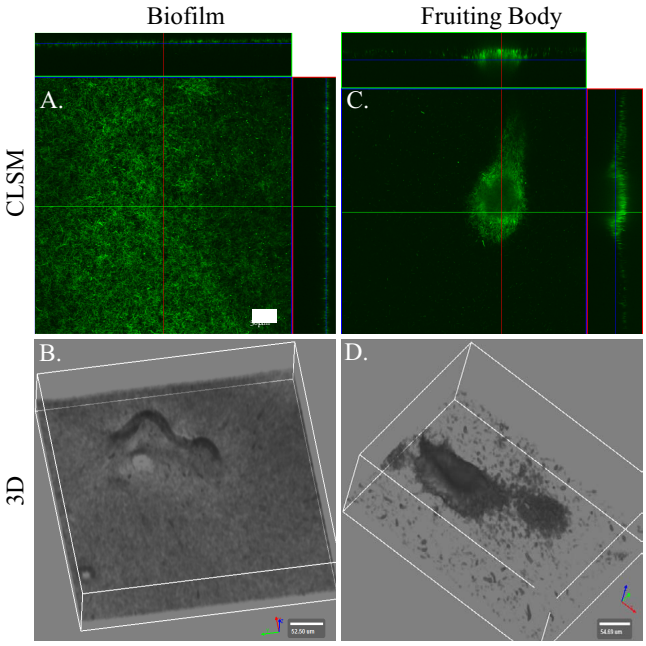

FIG 1 Fluorescence microscopy of *M. xanthus* flow cell growth and development. (A) Representative CLSM images of a 3-day-old *pilA-gfp*-labeled *M. xanthus* biofilm grown under vegetative conditions. Each image shows an orthogonal section of one layer of a z-stack collected for the representative structure by CLSM with a 20× objective, as described in the text. (B) Three-dimensional isometric images (3D) of architecture were generated from the same z-stack as the CLSM biofilm images in panel A, using Bisque (24). CLSM (C) and three-dimensional isometric (D) images for a 4-day-old *M. xanthus* fruiting body were produced similarly.

marked loss of the thick microbial mat, leaving behind a few peripheral rod cells surrounding the 4-day-old fruiting body structure (Fig. 1D). The concave appearance of the 3D rendering of the fruiting body is due to the loss of fluorescence recorded by CLSM in the interior of the structure due to loss of expression of *pilA-gfp* and the degradation of GFP in late fruiting body development (24, 28).

To demonstrate that the mature 4-day-old fruiting bodies were structurally similar to those previously observed, we stained the fruiting bodies with the fluorophore SPF, an alternative stain to calcofluor white (29), which has been used to visualize EPS (30). Observation of EPS deposition within the fruiting body by the use of SPF revealed uniform staining throughout the structure (see Fig. S3A and C in the supplemental material). This result paired with the results of differential interference contrast (DIC) microscopy (see Fig. S3B and D) demonstrates the presence of internal cellular structures and validates that fruiting bodies formed under these conditions are equivalent to those previously observed using standard conditions.

Time course studies of biofilm growth and developmental shifts. One of the advantages of culturing biofilms within flow cells and observing them under CLSM is the ability to image *M. xanthus* strains in real time over a period of days or even weeks. This allows for the monitoring of dynamic changes to the same structure under constant environmental conditions without disrupting or consuming the sample. It also allows for the monitoring of how the biofilm is established from inoculation to the establishment of a dense biofilm. We imaged *M. xanthus pilA-gfp*

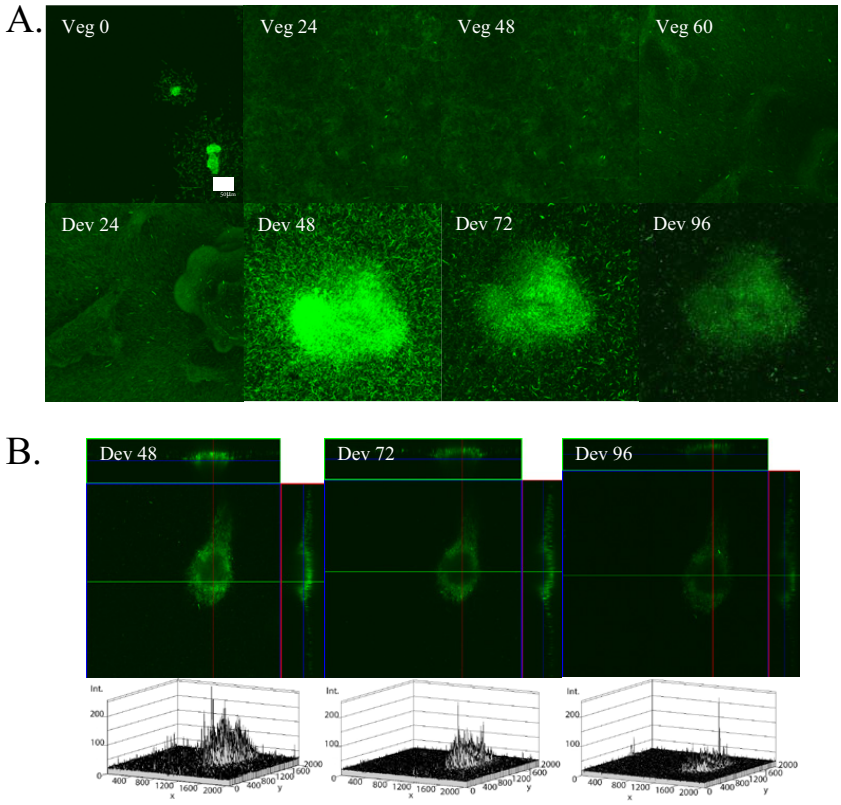

FIG 2 *M. xanthus* growth, development, and architecture in a flow cell over time. (A) Representative CLSM images of *pilA-gfp*-labeled *M. xanthus* grown under vegetative (Veg) conditions followed by a developmental switch (Dev). Time points are numbered relative to the end of the allowed attachment period (Veg 0) and were reset after the initiation of the developmental program (Dev 0). (B) Each image shows an orthogonal section of one layer of a representative z-stack of a second mature *pilA-gfp*-labeled *M. xanthus* fruiting body collected by CLSM with a 20× objective, as described in the text. Time points are numbered relative to the initiation of the developmental program. Architectural intensity representations generated from the z-stacks are reported below the corresponding images, where the *x* and *y* axes are arbitrary coordinates relative to the imaged fruiting body and the *z* axis is the relative intensity.

biofilm growth and development after sudden nutrient deprivation over a period of 1 week (Fig. 2A). The initial inoculum was allowed to adhere to the growth surface for 2 h, and then the vegetative time zero was imaged as the flow was turned on (Fig. 2A, Veg 0 panel). Biofilm growth was monitored until a stable confluent culture was reached, at 60 h (Fig. 2A, Veg 60 panel). At that point, the MC7 buffer was rapidly exchanged to trigger the developmental life cycle. Aggregates and mounds were observed 24 h after buffer exchange, and at 48 h, a single mature fruiting body was imaged every day for two more days (Fig. 2A, panels Dev 24 to Dev 96). Similarly, wild-type *M. xanthus* was monitored throughout the same time course by light microscopy (see Fig. S4 in the supplemental material) and was found to be roughly consistent in developmental timing to cells grown under submerged culture (31) and agar plate assay (28) conditions.

Architectural metrics were observed and recorded for mature fruiting bodies over a 3-day period (Fig. 2B). Briefly, GFP expression intensity was positionally determined for each image within the z-stack. These data were then averaged with the intensities for those images above and below to generate a quantitative representation of the fruiting body architecture. The fruiting body architecture detected in the flow cells was consistent with previously reported fruiting body structures grown under a variety of conditions, including submerged culture (31) and agar plate assay (28) conditions.

Fruiting body formation was also monitored to determine that the composition was in agreement with the hypothesis that development requires the interaction of tens of thousands of established cells to form complex aggregates (32). This was accomplished within the flow cell by observing the growth and development of biofilms comprising the mixed populations of two differentially marked *M. xanthus* strains. By mixing the *PpilA-gfp* transcriptional fusion strain with a nonfluorescent strain harboring the same antibiotic selection marker, we observed an even distribution of *gfp* expression within all observed fruiting bodies (see Fig. S5 in the supplemental material), which is indicative of *M. xanthus*'s multicellular behavior (32). Using two different ratios of cells, 1:1 and 1:5 (see Fig. S5), the fluorescence ratios for the fruiting bodies paralleled the ratios for input cells. Comparing the 1:1 and 1:5 ratios of *gfp* to non-*gfp* cells, we observed a GFP intensity difference of 6.39 ± 3.87 when fluorescence was measured directly, demonstrating that cells behaved as expected within the flow cell apparatus.

Differential cell staining of EPS. The ability to visualize cellular architecture via CLSM extends not only to fluorescent epitope-tagged strains but also to the use of cellular stains and markers. Much like the use of fluorescent tags, this can be done in real time, without fixation. This facilitates the use of multiple stains in order to discern colocalization. To examine this in *M. xanthus*, we established a confluent vegetative biofilm within the flow chamber,

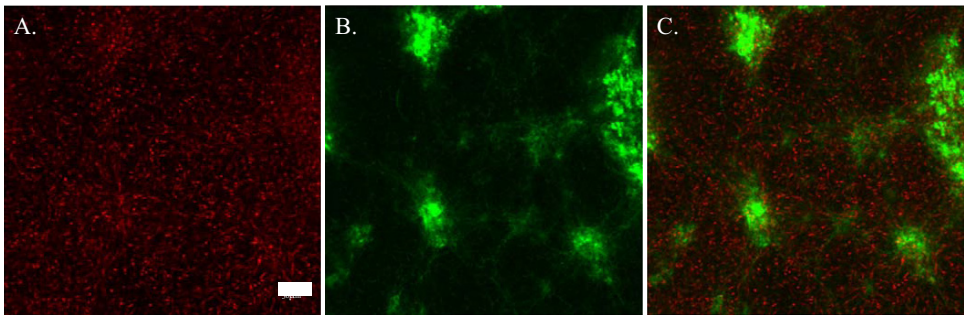

FIG 3 EPS deposition in *M. xanthus* biofilm. (A) Representative CLSM image of a confluent *M. xanthus* vegetative biofilm stained with the general cell stain Syto60. (B) The same frame imaged via CLSM and counterstained with the EPS-specific stain SPF. (C) Overlay of both the Syto60 and SPF images.

as described above, and subsequently stained the biofilm with Syto60 in order to visualize individual cells (Fig. 3A). EPS was stained with SPF, and the same frame was imaged in order to locate the deposition of EPS within the biofilm (Fig. 3B).

An overlay of the two images indicates a homogeneous confluent growth of the *M. xanthus* biofilm, with deposition of EPS in large patch-like regions beneath areas of what appear to be slightly denser *M. xanthus* concentrations (Fig. 3C). The same EPS deposition pattern was observed previously by Hu et al., suggesting that EPS is produced and secreted beneath *M. xanthus* swarms (33).

Nutrient titration to determine minimum concentration required for vegetative growth. In order to identify important nutrient sensors, we determined the minimum required nutrient concentration to maintain a vegetative lifestyle. For this reason, growth and development must be carried out in MOPS-based nutrient medium, as *M. xanthus* will not produce fruiting bodies under standard Tris-HCl-buffered medium conditions. To identify the nutrient concentration range that represents the boundary between the vegetative and developmental states, a nutrient titration was applied to a number of mature biofilms grown in parallel (Fig. 4).

Using a strain containing *gfp* transcriptionally coupled to the *devR* gene as a reporter, we can readily identify strains that have undergone development by both light and fluorescence microscopy (18). The biofilms under titration maintained a stable vegetative state even after a 250-fold reduction in the Casitone concentration (0.004%) from the concentration routinely used in standard vegetative growth (1%) (Fig. 4). Even after 4 days at 0.004% Casitone, no expression was observed from the *devR-gfp* fusion, and no physical signs of development were evident. This implied that even under these low-nutrient conditions, development was not simply delayed, but the cells were still in a vegetative state. It was not until the nutrient concentration was dropped another 2-fold, to 0.002%, that the developmental program was observed to be initiated. Under these conditions, the entire sample had undergone development by producing readily observable fruiting bodies that also showed a marked increase in fluorescence compared to the other cultures in the titration (Fig. 4). Within 24 h of the shift to 0.002% Casitone, fluorescence was detected from the *devR-gfp* transcriptional fusion, demonstrating that development was occurring in a manner temporally similar to that with standard starvation-inducing procedures (18). Similar results were observed via light microscopy, using the wild-type DK1622 strain, in a parallel experiment (see Fig. S6 in the supplemental material). Finally, it should be noted that similar results could be obtained when the flow rate was changed at these low nutrient levels. We observed not only that we could initiate fruiting body development by decreasing the input nutrient concentration from 0.004% to 0.002% but also that, if the flow rate was decreased while at a Casitone concentration of 0.004%, we could also induce

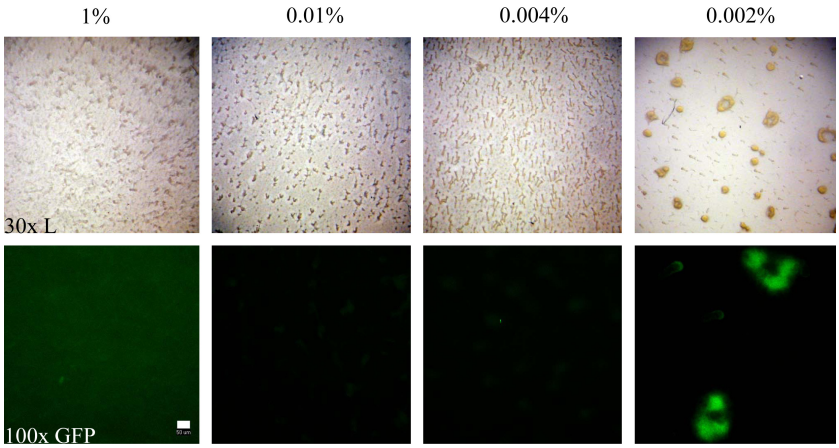

FIG 4 Nutrient titration of established *M. xanthus* biofilms. Representative light microscope images (L) and fluorescence microscope images (GFP) of a DK11239 biofilm titration series are shown for total magnifications of ×30 and ×100, respectively. Numbers represent the percentages of Casitone (in MC7 buffer) present after a nutritional shift for each of the flow cell biofilm cultures.

the developmental program (data not shown). This demonstrates that at low nutrient concentrations, our flow cell approach provides a variety of methods to manipulate the cells' perceived nutrient concentration.

DISCUSSION

The ability of *M. xanthus* to sense and respond to the environment is critical for the regulation of a number of key pathways leading toward adventurous and social motility, swarming, predation, and development. As with many pathways, but especially with development, understanding the mechanism by which the cell senses and responds to external stimuli can be a difficult task, one that has been ongoing for decades (34). This is further complicated in development when the pathways are regulated by a nutrient sensor(s) in a culture environment that is rapidly changing due to the consumption of nutrients and the deposition of bacterial waste/metabolites. In order to identify these early developmental nutrient sensors, we proposed the use of flow cells to ensure a constant controllable growth environment.

Flow cells provide a tractable environment for the study of *M. xanthus*. Until their employment in this study, the use of flow cells for the growth and maintenance of bacterial biofilms had yet to be applied to *M. xanthus*. Flow cells are versatile environments, allowing for the use of cellular and molecular techniques, as demonstrated by CLSM imaging. Live epitope tagging is readily observable within flow cells, as demonstrated with the *pilA-gfp* strain images (Fig. 1 and 2). While not tested in this study, multiple fluorescent epitope tags should also be readily observable, allowing for colocalization/expression studies. The aggregation and mature fruiting body architectural structure observed in our experiments are reminiscent of a previous study by Lux et al. (28) and are consistent with more recent investigations using infrared optical coherence tomography (35). Live macromolecular staining is also easily carried out within flow cells by simply injecting the stains to the desired concentration, followed by washing, as demonstrated in this study by staining for EPS (Fig. 3). This result is directly comparable to the work done by Hu et al. (14), as it was carried out under similar conditions (MOPS-buffered submerged vegetative culture) and with similar molecular stains (Syto9 and Alexa 633-wheat germ agglutinin).

Significance of the minimum nutrient concentration supporting vegetative growth. The use of flow cells provides a method of culturing *M. xanthus* that limits the possibility of unevenly exhausting the nutrients over time. This improvement over classic culturing methods, along with the ability to rapidly exchange medium without mechanically disturbing the culture, allowed us to identify the minimum nutrient concentration necessary for the maintenance of a vegetative biofilm. While this concentration has proven to be relative to the particular conditions used within our flow cells (data not shown), we can effectively control developmental responses not only via the nutrient concentration but also by the rate of nutrient replacement within the culture environment. Our ability to maintain a vegetative biofilm just above the developmental threshold (Fig. 4) will prove to be critical in our further studies of those sensors and early developmental triggers affected by the environmental nutrient concentration. The titration establishes a slow-growth steady state, which allows us to separate the expression of genes required for slow growth from that of genes required for the very earliest steps in the developmental program. In a way, this system allows us to increase the signal-to-noise ratio by establishing a vegetative steady state poised at the developmental nutrient threshold. The method developed here establishes the tools for investigation into the nutrient sensory systems as well as their dependent developmental pathways.

ACKNOWLEDGMENTS

This work was supported in part by National Science Foundation grant MCB-1024989 to M.S. and by National Institutes for Health, NIGMS, training grant 5T32GM007377-34 to D.L.W.

We thank Steven Lucero of the UC Davis Prototype Lab for the printing of single-chamber flow cells and Russell Neches for discussions on their design. We also thank Jonny Pham for help with the imaging of the titration and mixing experiments and Letal I. Salzberg for her comments on the manuscript.

REFERENCES

1. **Dworkin M, Kaiser D.** 1985. Cell interactions in myxobacterial growth and development. Science **230:**18–24. http://dx.doi.org/10.1126/science.3929384.
2. **Kaiser D.** 2004. Signaling in myxobacteria. Annu. Rev. Microbiol. **58:**75–98. http://dx.doi.org/10.1146/annurev.micro.58.030603.123620.
3. **Shimkets LJ.** 1987. Control of morphogenesis in myxobacteria. Crit. Rev. Microbiol. **14:**195–227. http://dx.doi.org/10.3109/10408418709104439.
4. **Shimkets LJ, Reichenbach H, Dworkin M.** 2005. The Myxobacteria. Springer, New York, NY.
5. **Wireman JW, Dworkin M.** 1977. Developmentally induced autolysis during fruiting body formation by Myxococcus xanthus. J. Bacteriol. **129:**798–802.
6. **O'Connor KA, Zusman DR.** 1988. Reexamination of the role of autolysis in the development of Myxococcus xanthus. J. Bacteriol. **170:**4103–4112.
7. **Whiteley M, Bangera MG, Bumgarner RE, Parsek MR, Teitzel GM, Lory S, Greenberg EP.** 2001. Gene expression in Pseudomonas aeruginosa biofilms. Nature **413:**860–864. http://dx.doi.org/10.1038/35101627.
8. **Branda SS, Gonzalez-Pastor JE, Dervyn E, Ehrlich SD, Losick R, Kolter R.** 2004. Genes involved in formation of structured multicellular communities by Bacillus subtilis. J. Bacteriol. **186:**3970–3979. http://dx.doi.org/10.1128/JB.186.12.3970-3979.2004.
9. **Branda SS, Chu F, Kearns DB, Losick R, Kolter R.** 2006. A major protein component of the Bacillus subtilis biofilm matrix. Mol. Microbiol. **59:**1229–1238. http://dx.doi.org/10.1111/j.1365-2958.2005.05020.x.
10. **Beenken KE, Dunman PM, McAleese F, Macapagal D, Murphy E, Projan SJ, Blevins JS, Smeltzer MS.** 2004. Global gene expression in Staphylococcus aureus biofilms. J. Bacteriol. **186:**4665–4684. http://dx.doi.org/10.1128/JB.186.14.4665-4684.2004.
11. **Gonzo EE, Wuertz S, Rajal VB.** 2012. Continuum heterogeneous biofilm model—a simple and accurate method for effectiveness factor determination. Biotechnol. Bioeng. **109:**1779–1790. http://dx.doi.org/10.1002/bit.24441.
12. **D'Alvise PW, Sjoholm OR, Yankelevich T, Jin Y, Wuertz S, Smets BF.** 2010. TOL plasmid carriage enhances biofilm formation and increases extracellular DNA content in Pseudomonas putida KT2440. FEMS Microbiol. Lett. **312:**84–92. http://dx.doi.org/10.1111/j.1574-6968.2010.02105.x.
13. **Taylor RG, Welch RD.** 2010. Recording multicellular behavior in Myxococcus xanthus biofilms using time-lapse microcinematography. J. Vis. Exp. **2010:**2038. http://dx.doi.org/10.3791/2038.
14. **Hu W, Lux R, Shi W.** 2013. Analysis of exopolysaccharides in Myxococcus xanthus using confocal laser scanning microscopy. Methods Mol. Biol. **966:**121–131. http://dx.doi.org/10.1007/978-1-62703-245-2_8.
15. **Palsdottir H, Remis JP, Schaudinn C, O'Toole E, Lux R, Shi W, McDonald KL, Costerton JW, Auer M.** 2009. Three-dimensional macromolecular organization of cryofixed Myxococcus xanthus biofilms as revealed by electron microscopic tomography. J. Bacteriol. **191:**2077–2082. http://dx.doi.org/10.1128/JB.01333-08.
16. **Kaiser D.** 1979. Social gliding is correlated with the presence of pili in Myxococcus xanthus. Proc. Natl. Acad. Sci. U. S. A. **76:**5952–5956. http://dx.doi.org/10.1073/pnas.76.11.5952.
17. **Welch R, Kaiser D.** 2001. Cell behavior in traveling wave patterns of myxobacteria. Proc. Natl. Acad. Sci. U. S. A. **98:**14907–14912. http://dx.doi.org/10.1073/pnas.261574598.

18. **Kaiser D.** 1999. Cell fate and organogenesis in bacteria. Trends Genet. **15:**273–277. http://dx.doi.org/10.1016/S0168-9525(99)01740-0.
19. **Kroos L, Kuspa A, Kaiser D.** 1986. A global analysis of developmentally regulated genes in Myxococcus xanthus. Dev. Biol. **117:**252–266. http://dx.doi.org/10.1016/0012-1606(86)90368-4.
20. **Berleman JE, Chumley T, Cheung P, Kirby JR.** 2006. Rippling is a predatory behavior in Myxococcus xanthus. J. Bacteriol. **188:**5888–5895. http://dx.doi.org/10.1128/JB.00559-06.
21. **Kuehn M, Hausner M, Bungartz HJ, Wagner M, Wilderer PA, Wuertz S.** 1998. Automated confocal laser scanning microscopy and semiautomated image processing for analysis of biofilms. Appl. Environ. Microbiol. **64:**4115–4127.
22. **Schneider CA, Rasband WS, Eliceiri KW.** 2012. NIH Image to ImageJ: 25 years of image analysis. Nat. Methods **9:**671–675. http://dx.doi.org/10.1038/nmeth.2089.
23. **Merod RT, Warren JE, McCaslin H, Wuertz S.** 2007. Toward automated analysis of biofilm architecture: bias caused by extraneous confocal laser scanning microscopy images. Appl. Environ. Microbiol. **73:**4922–4930. http://dx.doi.org/10.1128/AEM.00023-07.
24. **Kvilekval K, Fedorov D, Obara B, Singh A, Manjunath BS.** 2010. Bisque: a platform for bioimage analysis and management. Bioinformatics **26:**544–552. http://dx.doi.org/10.1093/bioinformatics/btp699.
25. **Klausen M, Heydorn A, Ragas P, Lambertsen L, Aaes-Jorgensen A, Molin S, Tolker-Nielsen T.** 2003. Biofilm formation by Pseudomonas aeruginosa wild type, flagella and type IV pili mutants. Mol. Microbiol. **48:**1511–1524. http://dx.doi.org/10.1046/j.1365-2958.2003.03525.x.
26. **Moller S, Sternberg C, Andersen JB, Christensen BB, Ramos JL, Givskov M, Molin S.** 1998. In situ gene expression in mixed-culture biofilms: evidence of metabolic interactions between community members. Appl. Environ. Microbiol. **64:**721–732.
27. **Jelsbak L, Sogaard-Andersen L.** 2003. Cell behavior and cell-cell communication during fruiting body morphogenesis in Myxococcus xanthus. J. Microbiol. Methods **55:**829–839. http://dx.doi.org/10.1016/j.mimet.2003.08.007.
28. **Lux R, Li A, Shi W.** 2004. Detailed three-dimensional analysis of structural features of *Myxococcus xanthus* fruiting bodies using confocal laser scanning microscopy. Biofilms **1:**293–303. http://dx.doi.org/10.1017/S1479050505001559.
29. **Hoch HC, Galvani CD, Szarowski DH, Turner JN.** 2005. Two new fluorescent dyes applicable for visualization of fungal cell walls. Mycologia **97:**580–588. http://dx.doi.org/10.3852/mycologia.97.3.580.
30. **Cowan SE, Gilbert E, Liepmann D, Keasling JD.** 2000. Commensal interactions in a dual-species biofilm exposed to mixed organic compounds. Appl. Environ. Microbiol. **66:**4481–4485. http://dx.doi.org/10.1128/AEM.66.10.4481-4485.2000.
31. **Kuner JM, Kaiser D.** 1982. Fruiting body morphogenesis in submerged cultures of Myxococcus xanthus. J. Bacteriol. **151:**458–461.
32. **Ward MJ, Zusman DR.** 1999. Motility in Myxococcus xanthus and its role in developmental aggregation. Curr. Opin. Microbiol. **2:**624–629. http://dx.doi.org/10.1016/S1369-5274(99)00032-6.
33. **Hu W, Hossain M, Lux R, Wang J, Yang Z, Li Y, Shi W.** 2011. Exopolysaccharide-independent social motility of Myxococcus xanthus. PLoS One **6:**e16102. http://dx.doi.org/10.1371/journal.pone.0016102.
34. **Bretscher AP, Kaiser D.** 1978. Nutrition of Myxococcus xanthus, a fruiting myxobacterium. J. Bacteriol. **133:**763–768.
35. **Harvey CW, Du H, Xu Z, Kaiser D, Aranson I, Alber M.** 2012. Interconnected cavernous structure of bacterial fruiting bodies. PLoS Comput. Biol. **8:**e1002850. http://dx.doi.org/10.1371/journal.pcbi.1002850.